Available online at www.sciencedirect.com

ScienceDirect

Geochimica et Cosmochimica Acta 313 (2021) 74–84

Geochimica et Cosmochimica Acta

www.elsevier.com/locate/gca

Iron-wüstite revisited: A revised calibration accounting for variable stoichiometry and the effects of pressure

M.M. Hirschmann

Dept. of Earth and Environmental Sciences, University of Minnesota, Minneapolis, MN 55455, USA

Received 28 May 2021; accepted in revised form 24 August 2021; Available online 1 September 2021

Abstract

We present thermodynamic and empirical calculations for the iron-wüstite (IW) buffer applicable from 100 kPa to 100 GPa and from 1000 to 3000 K. The thermodynamic calculation self-consistently accounts for changing stoichiometry of iron-saturated wüstite as a function of temperature and pressure. In contrast to some previous models for calculating IW at high pressure, the model incorporates a thermodynamically valid representation of the free energy of stoichiometric FeO at 100 kPa. Earlier high pressure models that relied on the JANAF thermochemical tables (Chase, 1998) were compromised because JANAF has erroneous values for the properties of FeO. This resulted in predicted oxygen fugacities buffered by IW that are between 0.2 and 1.1 log units too reducing at 3000 and 1000 K, respectively. The revised thermodynamic calculations indicate that iron-saturated wüstite becomes more nearly stoichiometric with increasing pressure, but that this shift depends on temperature. Near-stoichiometric FeO ($y < 0.01$, for $Fe_{1-y}O$) is reached close to 8 GPa at 1000 K and 17 GPa at 2000 K. An empirical function is presented that accurately reproduces the thermodynamic calculation and facilitates easy quantification of the f_{O2} of IW over the full range of temperatures and pressures covered by the model. Some caution is warranted in calculation of IW at high pressures, after FeO undergoes a transition from an insulator to a conductor and where low spin Fe^{2+} is stabilized, as the present model does not incorporate the effects of these transitions on the IW buffer.

Keywords: Iron; Wustite; Oxygen fugacity; Buffer; Redox

1. INTRODUCTION

The equilibrium coexistence of iron metal and wüstite, $Fe_{1-y}O$, (IW) fixes the oxygen fugacity according to the reaction

$$\underset{\text{metal}}{(1-y)Fe} + 1/2O_2 \Longleftrightarrow \underset{\text{wustite}}{Fe_{1-y}O} \quad (1)$$

and is an important reference buffer applied in earth and planetary science (Papike et al., 2005; Frost et al., 2008; Wadhwa, 2008). Although oxygen fugacities set by IW are significantly more reduced than those found for most rocks from Earth's crust and shallow mantle (Frost and Lindsley, 1991), they are relevant to conditions in the deep mantle (O'Neill et al., 1993; Frost et al., 2004; Rohrbach et al., 2007; Frost and McCammon, 2008), and in the Moon, Mars, and many meteorite parent bodies (Papike et al., 2005; Herd, 2008; Wadhwa, 2008). IW is also a critical reference buffer for processes of core formation in which silicate reacts with Fe-rich alloy (Frost et al. 2008). Further, in many experimental studies, the f_{O2} set by IW is used to quantify the f_{O2} through coexistence of FeO-bearing silicate with iron-precious metal (Pt, AuPd, Ir) alloys (Grove, 1981; Kessel et al., 2001; Medard et al., 2008; Barr and Grove, 2010; Stagno and Frost, 2010).

The f_{O2} set by the IW buffer at 100 kPa has been established to high accuracy by numerous studies from both metallurgists and earth scientists (Chipman and Marshall,

E-mail address: mmh@umn.edu

https://doi.org/10.1016/j.gca.2021.08.039
0016-7037/

1940; Darken and Gurry, 1945; Vallet and Raccah, 1964; Takayama and Kimizuka, 1980; Jacobsson and Rosen, 1981; Sjoden et al., 1986; O'Neill, 1988; O'Neill and Pownceby, 1993), but extension to high pressures requires equations of state of the condensed solids participating in the reaction, Fe metal and $Fe_{1-y}O$ oxide (Eugster and Wones, 1962; Campbell et al., 2009; Fischer et al., 2011b). An additional consideration is that the stoichiometry of $Fe_{1-y}O$ in equilibrium with Fe varies with temperature and pressure, and becomes essentially stoichiometric FeO ($y = 0$) at high pressure (McCammon and Liu, 1984; McCammon, 1993; Fei, 1996; Stølen and Grønvold, 1996; Seagle et al., 2008; Campbell et al., 2009). From this complication, two issues arise. First, in addition to an EOS needed to account for the effects of pressure, extension of calculated IW reaction to high pressure requires a valid thermodynamic representation for the properties of stoichiometric FeO at 100 kPa. Second, calculation of the f_{O2} set by IW at intermediate pressures, in which wüstite has stoichiometry between the equilibrium value prevailing at 100 kPa and FeO, requires accounting for the effect of stoichiometric variations on f_{O2}.

Eugster (1959) introduced the IW buffer to earth science and Eugster and Wones (1962) quantified the effects of pressure with a simple calculation employing the 100 kPa volumes of wüstite and Fe metal. Though this treatment does not account for changes in stoichiometry, it is a reasonable approximation for the modest effects of pressure in the crust and shallow mantle. This approach to calculating IW above 100 kPa persisted in the earth and planetary science community for nearly 50 years (e.g., Herd, 2008), until Campbell et al. (2009) and Fischer et al. (2011b) applied more advanced equations of state to allow extension to higher pressures.

Campbell et al. (2009) and Fischer et al. (2011b) conducted high pressure high temperature EOS measurements of coexisting Fe and FeO at pressures up to 200 GPa and used them to construct functions for IW applicable to deep planetary mantles. Because FeO is nearly stoichiometric at high pressure, Campbell et al. (2009) and Fischer et al. (2011b) calculated IW by combining their EOSs with the 100 kPa properties of FeO, taking the latter from the JANAF thermochemical tables (Chase, 1998). Between 1000 and 3000 K, the resulting low pressure functions for IW are between 0.9 and 0.2 log units more reduced than the well-established values for 100 kPa IW with equilibrium stoichiometry (e.g., O'Neill and Pownceby, 1993) (Fig. 1). These functions, thought to be valid above 5 GPa, do not address how IW should be interpolated at pressures between 100 kPa and 5 GPa, a region of considerable interest to processes such as basalt generation in shallow planetary mantles, or to calculation of f_{O2} in shallow magma oceans. For the latter, Zhang et al. (Zhang et al., 2017) assumed that between 100 kPa and 5 GPa, IW could be approximated by a simple linear interpolation between the high pressure and low pressure functions. More problematic, however, is that the properties of FeO given in the JANAF tables (Chase, 1998) are erroneous, as will be demonstrated below.

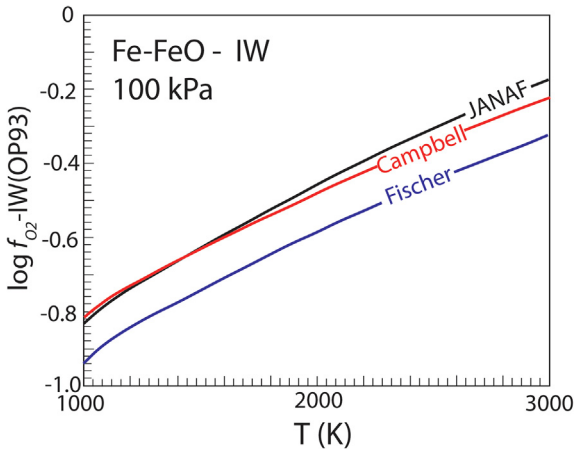

Fig. 1. Calculated log f_{O2} at 100 kPa as a function of temperature for Fe coexisting with stoichiometric FeO, from the JANAF thermochemical tables (Chase, 1998), Campbell et al. (2009) and Fischer et al. (2011b), relative to that calculated for the equilibrium iron-wüstite (IW) assemblage, from Pownceby and O'Neill (1993). JANAF (Chase, 1998) predicts conditions between 0.9 and 0.2 log units more reducing than IW; Campbell et al. (2009) and Fischer et al. (2011b), guided by the JANAF values, predict similar differences. However, as demonstrated in the text, the thermodynamic requirement is that stoichiometric Fe-FeO impose conditions more oxidizing than equilibrium IW.

Here we present a revised thermodynamic function for wüstite that self-consistently calculates $Fe_{1-y}O$ stoichiometry in equilibrium with iron as a function of temperature and pressure and gives values of f_{O2} that account for these changes. Additionally, we calibrate a revised empirical function for the f_{O2} buffered by the coexistence of Fe and equilibrium stoichiometry wüstite that is valid from 1000-3000 K and from 100 kPa to 100 GPa.

2. WÜSTITE THERMODYNAMICS AND THE PROPERTIES OF STOICHIOMETRIC FEO

IW is commonly calculated from empirical functions in which the stoichiometry of wüstite is implicit (e.g., Eugster and Wones, 1962; O'Neill, 1988; O'Neill and Pownceby, 1993; Herd, 2008), but these are based on data only from 100 kPa, where wüstite composition varies only slightly and remains far from stoichiometric. At high pressure and/or to treat wüstite stoichiometry explicitly, the f_{O2} buffered by the coexistence of pure iron metal and wüstite can be examined from the reaction

$$\underset{\text{metal}}{\text{Fe}} + 1/2\ \text{O}_2 \Longleftrightarrow \underset{\text{wustite}}{\text{FeO}} \qquad (2)$$

where $\underset{\text{wu stite}}{\text{FeO}}$ is the stoichiometric FeO endmember within an $Fe_{1-y}O$ wustite solid solution. Based on the equilibrium constant for reaction (2),

$$\left(G^0_{\text{FeO}} - 1/2G^0_{\text{O}_2} - G^0_{\text{Fe}}\right) = -\text{R}T\ln\frac{a^{\text{wustite}}_{\text{FeO}}}{a^{\text{metal}}_{\text{Fe}} f^{1/2}_{O_2}}, \qquad (3)$$

the oxygen fugacity can be calculated from

$$log\, f_{O_2} = \left(\frac{2}{\ln(10)}\right)\left[\left(G^0_{FeO} - 1/2G^0_{O_2} - G^0_{Fe}\right)/RT + \ln a^{wustite}_{FeO}\right], \quad (4)$$

where G^0_i are the standard state free energies of the components and $a^{wustite}_{FeO}$ is the activity of FeO in wüstite solid solution.

This approach requires specification of G^0_{FeO}as a function of temperature at 100 kPa, which has not been measured directly because FeO isn't stable at low pressure. Even if synthesized at high pressure or by some other means, thermodynamic measurement of stoichiometric FeO would present challenges, as it could decompose to Fe + $Fe_{1-y}O$ at high temperature in an EMF cell or calorimeter. For incorporation in the JANAF tables, Chase (1998) derived the properties of FeO crystal from those of FeO liquid, using the experimentally-derived enthalpy of fusion for non-stoichiometric wüstite (Coughlin et al., 1951). However, the properties they used for FeO liquid are based on an assumption unlikely to be correct. Describing their methodology for FeO liquid, Chase (1998) wrote (*p*. 1237),

"An assumption was made that during melting, the reaction

$Fe_{0.947}O(cr) = 0.947\ FeO\ (l) + (0.053/2)\ O_2\ (g)$ occurs."

Wüstite should not melt to stoichiometric FeO liquid, as the phase diagram determined by Darken and Gurry (1946) shows that above the melting point of wüstite, FeO is in the stability field of Fe metal and non-stoichiometric $Fe_{1-y}O$ liquid (Fig. 2). Further, the putative incongruent melting of wüstite should not yield O_2 gas, as wüstite stability is only viable at conditions far too reducing for such high O_2 fugacities. Thus, the properties of FeO liquid given in the JANAF tables (Chase, 1998) are inaccurate and this propagates to their derived properties of crystalline FeO.

A second reason that the JANAF properties of stoichiometric FeO solid are suspect is that the f_{O2} resulting from calculating the free energy change of the putative reaction

$$\underset{\text{metal}}{Fe} + 1/2\,O_2 \Longleftrightarrow \underset{\substack{\text{stoich.}\\ \text{oxide}}}{FeO}, \quad (5)$$

is more reduced than the f_{O2} for stable coexistence of Fe and equilibrium, non-stoichiometric wüstite (Eq. (2)). This accounts for the offset in f_{O2} between Campbell et al. (2009) and Fischer et al. (2011b) and low pressure IW calibrations (Fig. 1). Although it might seem sensible that stoichiometric FeO would impose conditions more reduced than wüstite with appreciable Fe^{3+}, this cannot be correct in the presence of Fe. Rather, the f_{O2} calculated from the Fe + FeO assemblage must be more oxidizing than equilibrium IW.

As the equilibrium assemblage must be that which has the lowest free energy at the conditions of interest, at low pressure the assemblage IW (Eq. (1)) must have a lower Gibbs free energy than an Fe-FeO assemblage (Eq. (5)). JANAF predicts incorrectly that the Fe-FeO assemblage has a lower free energy than equilibrium IW. This can be inferred by comparing the f_{O2} calculated for IW as compare to that calculated from an assumed Fe-FeO assemblage, as detailed in the following paragraphs.

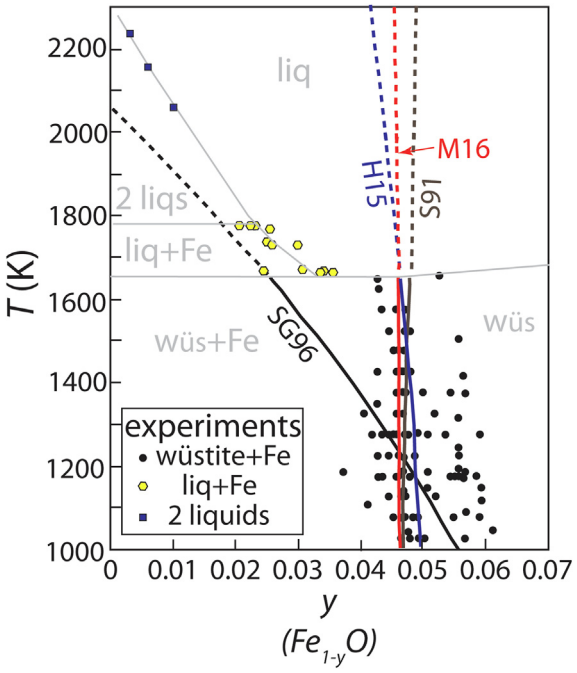

Fig. 2. Compositions of wüstite, $Fe_{1-y}O$ in equilibrium with Fe metal as a function of temperature at 100 kPa. Experimental compositions are from the compilation of Wriedt (1991). Also shown are iron-wüstite phase boundaries calculated from the thermodynamic models of Sundman (1991) (S91), Stølen and Grønvold (1996) (SG96), Hidayat et al. (2015) (H15), also used in this study, and Myhill (2016) (M16). Above the melting temperature of wüstite (1640 K, Coughlin et al., 1951), metastable extensions of the calculated Fe-$Fe_{1-y}O$ boundaries are shown as dashed curves. Except for Stølen and Grønvold (1996), which was calibrated only up to 1200 K and diverges from experimental bounds at high temperature, the thermodynamic models predict phase boundaries similar to each other and consistent with experimental observations. Also shown are experimental bounds on the composition of Fe-oxide liquid coexisting with Fe metal (Darken and Gurry, 1946), and with metallic liquid (Distin et al., 1971) demonstrating that wüstite cannot melt to liquid with FeO stoichiometry, as assumed by JANAF (Chase, 1998). Gray lines and phase assemblages indicate approximate additional phase boundaries after Distin et al. (1971) and Hidayat et al. (2015), though fields of coexisting wüstite + liquid above the solidus, required by the phase rule but unconstrained by experiment, are omitted.

Consider a bulk composition consisting of Fe and Fe-oxide at a particular pressure and temperature in the system Fe-O, with thermodynamic components Fe and O_2. This same bulk composition can consist either of the IW assemblage or a combination of Fe and pure FeO. The total free energy of each, G^j, is given by

$$G^{IW} = n^{IW}_{Fe}\mu^{IW}_{Fe} + n^{IW}_{O_2}\mu^{IW}_{O_2} \quad (6a)$$

$$G^{FeFeO} = n^{FeFeO}_{Fe}\mu^{FeFeO}_{Fe} + n^{FeFeO}_{O_2}\mu^{FeFeO}_{O_2} \quad (6b)$$

where n^j_i are the number of moles of component *i* in assemblage *j*, and $\mu^j_i$is the chemical potential of component *i* in assemblage *j*. Because both assemblages have the same bulk composition,

$$n_{Fe}^{FeFeO} = n_{Fe}^{IW} \tag{7a}$$

$$n_{O_2}^{FeFeO} = n_{O_2}^{IW} = n_{O_2} \tag{7b}$$

and because both are saturated in Fe,

$$\mu_{Fe}^{IW} = \mu_{Fe}^{FeFeO} \tag{8}$$

Therefore

$$G^{IW} - G^{FeFeO} = n_{O_2}\left(\mu_{O_2}^{IW} - \mu_{O_2}^{FeFeO}\right), \tag{9}$$

As IW is the equilibrium assemblage,

$$G^{IW} < G^{FeFeO} \tag{10}$$

and so, because n_{O_2}must be a positive number,

$$\mu_{O_2}^{IW} < \mu_{O_2}^{FeFeO} \tag{11}$$

Finally, as

$$\mu_{O_2} = G_{O_2}^0 + RT\ln f_{O_2}, \tag{12}$$

$$f_{O_2}^{IW} < f_{O_2}^{FeFeO}. \tag{13}$$

Therefore, as illustrated in Fig. 3, the f_{O2} of equilibrium IW must be less than for the disequilibrium Fe-FeO assemblage at 100 kPa. JANAF (Chase, 1998) predicts that the f_{O2} of the Fe-FeO assemblage is less than that of IW (Fig. 1), which Fig. 3 shows must be incorrect if $G^{IW} < G^{FeFeO}$. Therefore, Campbell et al. (2009) and Fischer et al. (2011b) predict f_{O2}s that are at least 0.9–0.2 log units too reducing at 100 kPa across the temperature interval 1000–3000 K (Fig. 1). This inaccuracy propagates to f_{O2} calculated at high pressure.

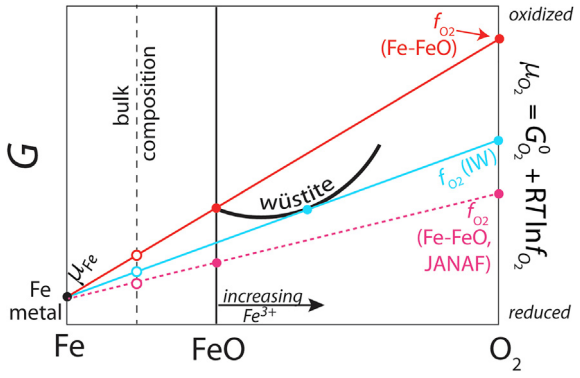

Fig. 3. Schematic *G-X* diagram for the system Fe-O with components Fe and O_2, showing that iron coexisting with the equilibrium non-stoichiometric wüstite must impose a more reduced oxygen fugacity (lower f_{O2}) than that coexisting with stoichiometric FeO, even though the wüstite has significant Fe^{3+}. For a given bulk composition, indicated by the vertical dashed line, the lowest free energy is obtained for Fe metal coexisting with equilibrium non-stoichiometric $Fe_{1-y}O$, and the resulting chemical potential of oxygen, μ_{O2}, is represented by linear projection to the O_2 component. Fe metal coexisting with pure FeO would produce a higher free energy and the corresponding μ_{O2} would be higher, and therefore more oxidized. Also shown is the relationship implied by JANAF (Chase, 1998), which predicts coexisting Fe and stoichiometric FeO imposes an f_{O2} more reduced than IW (Fig. 1). This cannot be correct, as it requires that Fe-FeO, rather than IW, be the equilibrium assemblage, and proves that G_{FeO} from JANAF is erroneously low.

To better understand the properties of $Fe_{1-y}O$ solution and how they may be accurately extrapolated to stoichiometric FeO, we compared 4 different thermodynamic models for wüstite (Sundman, 1991; Stølen and Grønvold, 1996; Hidayat et al., 2015; Myhill et al., 2016). The wüstite models of Kowalski and Spencer (1995) and Fabrichnaya and Sundman (1997), in common use in both earth science and metallurgy, are effectively identical to that of Sundman (1991). All of the thermodynamic models considered predict thermodynamic properties of end-member FeO. These necessarily are products of extrapolation and are interdependent with other model parameters, including the way that entropies of mixing and excess free energy terms are treated. However, if the models successfully predict multiple types of experimental observations across the range of compositional stability of wüstite, the extrapolated properties of FeO can be considered to be reasonably constrained. We examined the models for their accuracy with respect to (a) their ability to predict wüstite composition along the iron-wüstite phase boundary (Fig. 2) (b) their ability to predict wüstite composition along the wüstite-magnetite phase boundary (c) the accuracy of the f_{O2} calculated for IW, compared to experimental measurements (Fig. 4) (d) the accuracy of the relationship between wüstite stoichiometry verses f_{O2} in the wüstite stability field in between the bounding reactions with iron and magnetite. All of the models examined except that of Stølen and Grønvold (1996) reproduce these experimental constraints with high accuracy. And though none of them account for effects of short-range ordering or of vacancies on the anion site, complexities in the wüstite solution that can influence thermodynamic properties (Gavarri and Carel, 2019), their accuracy in reproducing diverse experimental constraints suggest that they can be extrapolated to stoichiometric FeO with confidence.

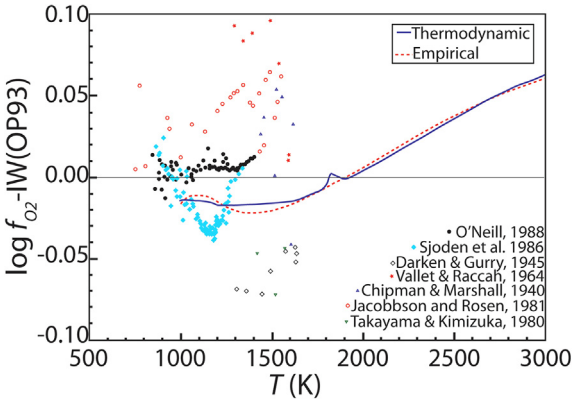

Fig. 4. Comparison of thermodynamic and empirical calculations of the IW buffer at 100 kPa from this work versus selected experimental studies (Chipman and Marshall, 1940; Darken and Gurry, 1945; Jacobsson and Rosen, 1981; O'Neill, 1988; Sjoden et al., 1986; Takayama and Kimizuka, 1980; Vallet and Raccah, 1964), both compared and referenced to the empirical parameterization of O'Neill and Pownceby (1993) (OP93). The kink in the thermodynamic calculation near 1800 K is owing to a discontinuity in the Gibbs function for *bcc* iron near its melting point (1811 K).in the SGTE database (Dinsdale, 1991).

As illustrated in Fig. 5, all of the wüstite thermodynamic models examined fulfill the requirement that equilibrium wüstite coexisting with Fe impose lower f_{O2} than FeO and Fe. Also, all predict f_{O2} values for Fe + FeO within a narrow interval (±0.05 log units) and values for IW close to those given by high-accuracy models such as O'Neill and Pownceby (1993). Given that these employ different relations for the entropies and excess free energies of mixing, we take this agreement to affirm the accuracy of the extrapolated thermodynamic properties of FeO.

Among the models examined, we selected Hidayat et al. (2015) for the calculations that follow. Hidayat et al. (2015) reproduce the experimental measurements noted in the previous paragraph as well or better than the two models not selected (Myhill et al., 2016; Sundman, 1991), but as a practical matter, application of any of these three would yield nearly indistinguishable results. However, we favored Hidayat et al. (2015) because they examined multiple candidate entropy of mixing models and selected that which best fit all the experimental data, including heat capacities and 3rd law entropies of wüstite with variable stoichiometry.

3. CALCULATIONS

3.1. Wüstite stoichiometry and IW

To calculate the f_{O2} imposed by the stable coexistence of Fe and wüstite as a function of temperature and pressure, we employ the model of Hidayat et al. (2015), which treats wüstite as a solution between FeO and $FeO_{1.5}$. Details of the end-member properties are given in Tables S1 and S2, and the solid solution model described in the Appendix A. Cast with these endmembers, the condition defining the stoichiometry of wüstite in equilibrium with Fe is given by the reaction

$$\underset{\text{metal}}{\text{Fe}} + 2 \quad \underset{\text{wustite}}{\text{FeO}_{1.5}} \iff \underset{\text{wustite}}{3\text{FeO}} \tag{14}$$

and

$$\left(3G^0_{FeO} - 2G^0_{FeO_{1.5}} - G^0_{Fe}\right) + \mathrm{R}T\ln\left(a^3_{FeO}/a^2_{FeO_{1.5}}\right) = 0 \tag{15}$$

For the resulting wüstite composition in equilibrium with iron, the f_{O2} of IW is derived from the reaction

$$\underset{\text{wu stite}}{\text{FeO}} + 1/4\text{O}_2 \iff \underset{\text{wustite}}{\text{FeO}_{1.5}} \tag{16}$$

and

$$\log f_{O_2} = [4/\mathrm{R}T\ln(10)]\left[\left(G^0_{\mathrm{FeO}_{1.5}} - G^0_{FeO} - 1/4G^0_{O_2}\right) + \mathrm{R}T\ln\left(a_{\mathrm{FeO}_{1.5}}/a_{\mathrm{FeO}}\right)\right]. \tag{17}$$

In cases where Fe and wüstite are in equilibrium, Eqs. (4) and (17) return the same oxygen fugacity, but Eq. (4) can be applied when Fe and wüstite or FeO coexist without being in equilibrium (e.g., Figs. 3 and 5) and Eq. (17) can be applied for wüstite that is not saturated in Fe, for example, in the wüstite-only field between the Fe metal and magnetite phase boundaries.

For the calculation of free energies of O_2 and the Fe polymorphs *fcc* (γ Fe), *bcc* (α Fe and δ Fe) and *hcp* (ε Fe), we use the SGTE database of properties of pure elements (Dinsdale, 1991) (Table S1). The SGTE database is widely adopted in the metallurgical literature and consistent with many subsequent studies (Sundman, 1991; Kowalski and Spencer, 1995; Fabrichnaya and Sundman, 1997; Komabayashi, 2014), including Hidayat et al. (2015).

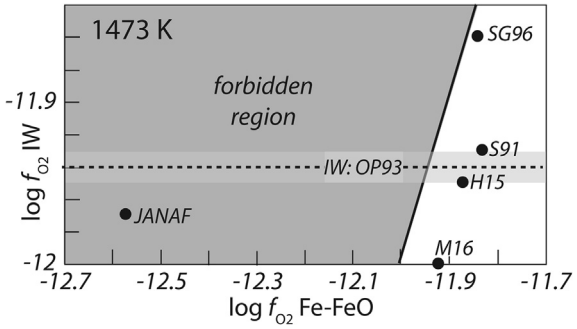

Fig. 5. Calculated log f_{O2} at 100 kPa and 1473 K for Fe metal coexisting with stoichiometric FeO and with equilibrium non-stoichiometric wüstite from JANAF (Chase, 1998) and from the wüstite solution models of Sundman (1991), Stølen and Grønvold (1996) ,Hidayat et al. (2015), and Myhill et al. (2016). For the thermodynamic models, the equilibrium wüstite composition is calculated self-consistently. For JANAF, the wüstite is for $Fe_{0.947}O$, comparable to the equilibrium composition at 1473 K (Fig. 2). All the solution models plot to the right of the 1:1 line, showing that they are consistent with the thermodynamic requirement that f_{O2} for Fe-wüstite is lower than for Fe-FeO (Fig. 3), but JANAF is not. Also shown is the equilibrium f_{O2} for IW from O'Neill and Pownceby (1993) (OP93), showing the correspondence to the predictions of the solution models.

3.2. Extension to high pressure

To calculate the properties of iron and iron oxide at high pressure, we use the models of Komabayashi (2014), who employed a universal (Vinet) EOS for isothermal compression combined with an Anderson-Grüneisen treatment of thermal pressure for FeO and Fe metal (See Appendix A). Komabayashi (2014) reproduces experimental *P-V-T* measurements of Fe and FeO, including those from Campbell et al. (2009) and Fischer et al. (2011b), up to 360 and 220 GPa, and is consistent with the experimental phase diagrams for Fe and FeO.

Komabayashi (2014) provides EOS constraints for stoichiometric FeO, but no guidance for the thermoelastic properties of Fe^{3+}-bearing wüstite. Extension of the Hidayat et al. (2015) thermodynamic model for wüstite to high pressure requires EOS applicable to $FeO_{1.5}$. As $FeO_{1.5}$ is a fictive endmember, located well past the stability limit of actual wüstites (i.e, considering wüstite as $Fe_{1-y}O$, $y = 0.3333$ for $FeO_{1.5}$ whereas the limit of wüstite stability is near $y = 0.12$; Fig. S1), the EOS properties must be extrapolated from less Fe^{3+}-rich materials. As elaborated in the Appendix A, we extrapolated the reference volume, V_0, from wüstite of variable composition (Fig. S1) and took the bulk modulus, K_0, to be compositionally invariant (Fig. S2), as also concluded by Stølen and Grønvold

(1996), Fei (1996) and Haavik et al. (2000). Other parameters in the EOS are also assumed to be constant (Table S2).

For Fe metal, Komabayashi (2014) did not consider the EOS parameters of the *bcc* phase, so we adopt a value of V_0 (Table S2) consistent with Dorogokupets et al. (2017) and EOS parameters otherwise the same as for *fcc* iron. Because *bcc* is only stable at low pressure, refined values of its bulk modulus and thermal expansion have little impact on either phase diagram or f_{O2} calculations. The resulting calculated fields of Fe polymorph stability are given in Table S3. For FeO, the calculations are valid for the cubic B1 high spin phase of FeO. Where the rhombohedral B1 or B8 polymorphs are stable at high pressure and low temperature (Ozawa et al., 2010), we do not present calculated values of f_{O2} (Table S4). An additional important consideration is the effect of the transition of wüstite to a metallic phase and the stabilization of low spin Fe^{2+} at high pressure (Badro et al., 2003; Holmström and Stixrude, 2015) and this is examined further in the Discussion.

The calculated IW buffer is strictly applicable to equilibrium coexistence of crystalline iron and iron oxide. However, it is also possible to calculate the f_{O2} defined by the crystalline IW buffer above the melting temperatures of FeO and/or Fe. At these conditions, the metastable IW buffer is defined by the crystalline polymorph of Fe that has the lowest free energy at that P and T. Application of a solid–solid buffer to metastable conditions is standard practice in petrology, as for example, the characterization of basaltic magmas relative to the quartz-fayalite-magnetite buffer above the melting point of fayalite (1477 K at 100 kPa; Stebbins and Carmichael, 1984).

4. RESULTS

Calculated stoichiometry of $Fe_{1-y}O$ and f_{O2} of the IW buffer are given in increments of 1 GPa and 20 K from 100 kPa to 100 GPa and from 1000-3000 K in Tables S4 and S5, respectively. At 100 kPa these mirror those obtained by Hidayat et al. (2015) and are compared to experimental constraints in Figs. 2 and 4. To facilitate comparison, the IW experiments and calculation are referenced to the widely-adopted and precise 100 kPa function of O'Neill and Pownceby (1993). The calculated f_{O2} is consistent with experimental measurements and with the O'Neill and Pownceby (1993) parameterization to within 0.02 log units up to 2000 K (Fig. 4). At high temperature, the models diverge slightly, amounting to 0.06 log units at 3000 K. This difference is attributable to the stabilization of the *bcc* Fe polymorph at high temperature. The O'Neill and Pownceby (1993) model, calibrated only to 1644 K, does not account for the high temperature transition from *fcc* to *bcc* iron. Consequently, the present calculation is considered to be more accurate for extrapolation to high temperature. Predicted f_{O2}s for IW at high pressure are considered in the Discussion.

Calculations indicate that wüstite in equilibrium with Fe metal becomes more nearly stoichiometric FeO with increasing pressure (Fig. 4). At 1000 K, y diminishes from 0.05 at 100 kPa to 0.007 at 10 GPa and only 0.001 at 20 GPa. The decrease is more gradual at higher temperatures. For example, at 2000 K, y is 0.026 at 10 GPa and 0.007 at 20 GPa. The trend towards more stoichiometric wüstite with increasing pressure is in qualitative agreement with the prediction of Stølen and Grønvold (1996), which indicated that values of y at 1200 K are reduced to zero above 5 GPa.

5. EMPIRICAL CALCULATION OF IW TO 3000 K AND 100 GPA

To facilitate ready calculation of IW, we fit the thermodynamically calculated oxygen fugacity imposed by the coexistence of solid Fe and $Fe_{1-y}O$ to empirical functions from 1000-3000 K and 0.0001 to 100 GPa. Two separate functions are provided (Table 1), a low pressure fit for conditions in which *fcc* or *bcc* Fe are stable (or metastable with respect to Fe liquid) and a high pressure version in the field of stability of *hcp* Fe. The two are applicable below and above the calculated pressure of the *fcc-hcp* boundary, which between 1000 and 3000 K and 0.0001 and 100 GPa is given by the function

$$P(GPa) = x_0 + x_1 T + x_2 T^2, \quad (18)$$

where $x_0 = -18.64$, $x_1 = 0.04359$, and $x_2 = -5.069 \times 10^{-6}$ and T is in Kelvins.

Over the full range of temperatures and pressures, the empirical function matches the underlying thermodynamic calculation with an r.m.s. of 0.0065 log units and the largest deviation over the calculation space is 0.028 log units. At 100 kPa, the resulting empirical and thermodynamic functions differ with an r.m.s. of 0.0024 and a maximum deviation of 0.0077 log units. The 100 kPa portion of the function fits experimental data with an accuracy comparable to other high precision IW parameterizations (Fig. 4) (e.g., O'Neill, 1988; O'Neill and Pownceby, 1993) and is therefore appropriate for application to low pressure conditions.

Empirically calculated log f_{O2} values are tabulated from 0.001 to 100 GPa and 1000 to 3000 K and at intervals of 1 GPa and 20 K in Table S6. Also included (Table S7) is a spreadsheet calculator that facilitates calculation of IW from the empirical functions at user-supplied temperatures and pressures.

6. DISCUSSION

6.1. Comparison to IW calculated from previous high pressure parameterizations

The f_{O2} calculated for IW from the revised model indicates conditions systematically more oxidizing than those resulting from the models of Campbell et al. (2009) and Fischer et al. (2011b) (Fig. 7), with the largest differences (0.9–1.1 log units) at 1000 K and smaller differences (0.2–0.4) at 3000 K. At 2000 K the offset is 0.4–0.7 log units. These offsets largely follow the 100 kPa trend depicted in Fig. 1. Additional distinctions with increasing pressure derive from slightly different quantitative predictions from the respective EOSs, particularly at higher pressures.

Table 1
Empirical expressions for calculating IW between 1000 and 3000 K, 100 kPa-100 GPa. For *fcc* and *bcc* iron: $\log f_{O2} = \mathbf{a} + \mathbf{b}\,T + \mathbf{c}\,T \ln T + \mathbf{d}/T$. For *hcp* iron: $\log f_{O2} = \mathbf{e} + \mathbf{f}\,T + \mathbf{g}\,T \ln T + \mathbf{h}/T$. For each parameter $\mathbf{m}$ in equations above, $\mathbf{m} = \mathbf{m_0} + \mathbf{m_1}\,P + \mathbf{m_2}\,P^2 + \mathbf{m_3}\,P^3 + \mathbf{m_4}\,P^{1/2}$.

	0	1	2	3	4
***fcc* and *bcc* iron:**					
a	6.844864	1.175691 E−01	1.143873 E−03	0	0
b	5.791364 E−04	−2.891434 E−04	−2.737171 E−07	0	0
c	−7.971469 E−05	3.198005 E−05	0	1.059554 E−10	2.014461 E−07
d	−2.769002 E+04	5.285977 E+02	−2.919275 E+00	0	0
***hcp* iron:**					
e	8.463095	−3.000307 E−03	7.213445 E−05	0	0
f	1.148738 E−03	−9.352312 E−05	5.161592 E−07	0	0
g	−7.448624 E−04	−6.329325 E−06	0	−1.407339 E−10	1.830014 E−04
h	−2.782082 E+04	5.285977 E+02	−8.473231 E−01	0	0

Units: T: Kelvins, P: GPa. r.m.s. 0.00647 log units. Maximum mismatch 0.0283 log units.
Use *hcp* iron when P (GPa) > $\mathbf{x_0} + \boldsymbol{x_1}\,T + \mathbf{x_2}\,T^2$, where $\boldsymbol{x_0}$ = -18.64, $\boldsymbol{x_1}$ = 0.04359, and $\boldsymbol{x_2}$ = -5.069 × 10^{-6}. This parameterization is robust in interpolation between the temperature and pressure bounds given. It extrapolates smoothly to higher temperature, though not calibrated above 3000 K. Extrapolation to lower temperatures (<1000 K) or higher pressures (>100 GPa) is not recommended.

The simple formulation employed by Eugster and Wones (1962), in which the effects of pressure are attributed to a single constant, remains reasonably accurate at low pressures, particularly at high temperature, but diverges significantly at high pressure. For example, at 1500 K and above, it differs from the present model by no more than 0.1 log units up to near 10 GPa, after which the differential compressibilities of Fe and wüstite become important and the predicted f_{O2}s become too oxidized (Fig. 7).

6.2. Wüstite stoichiometry at high pressure and impact on IW

The calculated trend in wüstite stoichiometry versus pressure (Fig. 6) is intermediate between those reported from wüstite crystals retrieved from multianvil experiments at 1273 K (McCammon, 1993) and measured *in situ* in synchrotron multianvil experiments at 873–1273 K (Campbell et al., 2009). In the former, values of y remained close to 0.02 at 10–18 GPa, whereas the latter indicated nearly stoichiometric wüstite between 4 and 10 GPa (Fig. 4). These differing experimental results are not mutually compatible, and they may reflect partial disproportionation of retrieved wüstite during quenching. Seagle et al. (2008) retrieved nearly stoichiometric wüstite crystals (y = 0.994 ± 0.006) from diamond anvil cell (DAC) experiments between 19–93 GPa, perhaps owing to the more rapid quench of the DAC. Unfortunately, Seagle et al. (2008) did not record the final pressure imposed on the retrieved crystals prior to quench. (C. Seagle, writt. com, January 2021).

The predicted retention of small amounts of Fe^{3+} in wüstite at high pressure equilibrium with Fe metal is also consistent with experiments on ferropericlase solid solu-

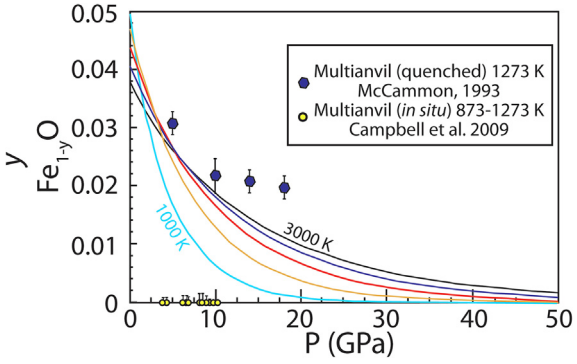

Fig. 6. Calculated stoichiometry, y, of $Fe_{1-y}O$ wüstite as a function of pressure, with curves in 500 K increments from 1000 K to 3000 K. Wüstite becomes more nearly stoichiometric at high pressure, but the effect is more gradual at higher temperature. Also shown are the experimentally-determined compositions of wüstite quenched and recovered from multianvil experiments (McCammon, 1993), with assumed pressure uncertainties of 1 GPa, and compositions of wüstite observed by *in situ* XRD in synchrotron multianvil experiments (Campbell et al. 2009), with NaCl pressure monitors. The latter were reported to be stoichiometric FeO based on lattice parameter determinations. As these are also affected by pressure, the uncertainties in y were estimated from the pressure uncertainties and the relationship between wüstite volume and stoichiometry (Fig. 2).

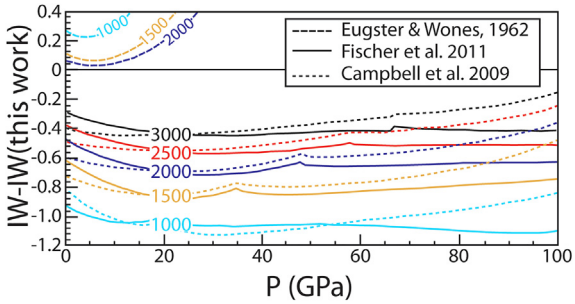

Fig. 7. Difference between IW log f_{O2} calculated from the present model and those calculated from Eugster and Wones (1962), Campbell et al. (2009), and Fischer et al. (2011b) as a function of temperature and pressure. The simple 1-parameter pressure term of Eugster and Wones (1962) reproduces the present model within 0.1 log units up to 10 GPa, but then diverges to more oxidizing conditions at higher pressures. The models of Campbell et al. (2009) and Fischer et al. (2011b) are offset to more reduced conditions: at 1000 K, with differences of 0.8–1.1 log units and at 3000 K they diminish to 0.2–0.4 log units. The kinks evident in these curves mark the transition from *fcc* to *hcp* iron.

tions coexisting with metal that indicate the persistence of Fe^{3+}. Otsuka et al. (2013) reported 1–2% Fe^{3+} from ferropericlase coexisting with FePt alloy recovered from multianvil experiments up 24 GPa, with Fe^{3+} concentrations increasing with Fe/(Fe + Mg), though considerable alloying Pt concentrations (>50 wt.%) enforced conditions somewhat more oxidizing than saturation with pure Fe. Frost et al. (2001) reported a similar trend of increasing Fe^{3+} with Fe/(Fe + Mg) for ferropericlase coexisting with iron at 15–23 GPa, though the reported Fe^{3+} concentrations were not clearly above detection limits.

Resolution of discrepancies between experiments and better evaluation of the accuracy of the thermodynamically-predicted stoichiometry-pressure trend awaits further developments, but fortunately, the shifts in stoichiometry with pressure are not likely to have large effects on the f_{O2} imposed by coexisting wüstite and iron. The analysis presented in Fig. 5 suggests that for accurate wüstite solution models, the f_{O2} imposed by Fe coexisting with wüstite has only a small dependence on stoichiometry. At 1473 K, models of Sundman (1991), Hidayat et al. (2015), and Myhill et al. (2016) all indicate that iron coexisting with equilibrium wüstite ($y \approx 0.05$) and with stoichiometric FeO differ in imposed f_{O2} by no more than 0.1 log units. These small differences require that the *G-X* curve of wüstite solid solution through this compositional interval describes a trend that is nearly parallel to the tangent line defined by the equilibrium assemblage of Fe + wüstite. Consequently, the shifts in wüstite stoichiometry from 100 kPa to higher pressure have only small effects on the f_{O2} of the IW buffer, and the uncertainties in the quantitative relationship between pressure and wüstite stoichiometry are of secondary importance to defining the f_{O2} of IW.

6.3. Effects of the insulator/conductor and high spin/low spin transitions in wüstite.

At pressures applicable to Earth's lower mantle, wüstite and ferropericlase transform from insulators to a metallic phase and the Fe^{2+} goes from the high spin to low spin state (Badro et al., 2003; Lin et al., 2007; Fischer et al., 2011a; Ohta et al., 2012; Holmström and Stixrude, 2015). The precise onset of these transitions and the relationships between the conductor/metallic and high spin/low spin states are not firmly established, though it appears that the insulator/conductor and high spin/low spin boundaries are distinct phase transitions (Lin et al., 2007). Based on enhanced electrical conductivity, the metallization transition begins near 30 GPa at 2500 K and at 90 K at 1500 K (Ohta et al., 2012), but emissivity measurements suggest a smaller effect of temperature, with the boundary at 50 GPa and 2700 K and at 75 GPa and 1300 K (Fischer et al., 2011a). The observation of a negative P-T slope for the insulator/conductor transition indicates that it is distinct from the high spin-low spin transition, which should have a positive slope, owing to expected reductions in both entropy and volume associated with the latter (Holmström and Stixrude, 2015). Low spin Fe^{2+} stabilizes FeO compared to its metastable high spin equivalent (Badro et al., 2003) and consequently the f_{O2} buffered by coexisting Fe and wüstite containing low spin Fe^{2+} should be more reduced than that calculated from a thermodynamic model that accounts only for high spin Fe^{2+}. This stabilizing effect is illustrated by enhanced partitioning of Fe^{2+} into ferropericlase coexisting with bridgmanite at high pressure, though experiments and theoretical calculations regarding the magnitude and locus in *P-T* space of Fe-enrichment in ferropericlase are not in full agreement (Badro et al., 2003; Piet et al., 2016; Prescher et al., 2014; Xu et al., 2017).

Though the effect of the insulator-conductor transition on *P-V-T* relations of FeO was found to be small, Fischer et al. (2011a) refit the data from Campbell et al. (2009) and Fischer et al. (2011b) to calibrate distinct EOS parameters for insulating and metallic FeO. To do so, they assumed that V_0 for metallic FeO is 0.5% smaller than for the insulator, and regressed fits to other EOS parameters (K_T, K', Grüneisen parameter), yielding values for both phases that are similar within statistical uncertainty. The influence of the insulator-conductor transition on FeO entropy, which should be evident from differences in the Grüneisen parameter, may not be well-resolved from existing *P-V-T* data.

As the locus and nature of the insulator/conductor and high spin/low spin transitions in FeO are not well constrained and because their effects on FeO thermodynamics remain poorly quantified, the present calibration does not incorporate their influence on calculated values of IW. To the extent that these transitions are not fully accommodated in a single EOS for FeO, calculated oxygen fugacities buffered by the coexistence of crystalline Fe and insulating high spin FeO may be less accurate when the conducting and/or low spin phases are stabilized. Beyond this limit, the calculated iron wüstite buffer may be taken as a metastable reference frame for oxygen fugacity, recognizing that experimental or natural coexistence of Fe and FeO at higher pressures could impose conditions that are more reduced. Improved accuracy of the IW buffer above 30–50 GPa will require accounting for the thermodynamic properties of metallized FeO.

7. CONCLUSIONS

This work provides a self-consistent calculation of the oxygen fugacity buffered by the coexistence of iron and wüstite that accounts both for effects of pressure and changing wüstite stoichiometry. It corrects previous inaccuracies that stemmed from adoption of properties of stoichiometric FeO from the JANAF thermochemical tables (Chase, 1998), a source that is generally considered to be highly reliable, but in this case has apparently erroneous values. We provide an empirical parameterization and a readily usable calculator that will facilitate quantification of oxygen fugacities in deep planetary mantles and in high pressure experiments.

Declaration of Competing Interest

The authors declare that they have no known competing financial interests or personal relationships that could have appeared to influence the work reported in this paper.

ACKNOWLEDGEMENTS

This work supported by NSF grant EAR2016215 and NASA grant 80NSSC19K0959. I thank T. Komabayashi, R. Myhill, and C. Seagle for correspondence that aided understanding of their published models and experiments, and to A.C. Withers for insightful and motivating discussions. Constructive reviews from M. Anenburg, R. Myhill, and an anonymous referee improved this work considerably, as did comments from Associate Editor Bernard Charlier. Thanks to Sanath Aithala for beta-testing the MATLAB scripts, though of course, any errors are the responsibility of the author.

APPENDIX A

Thermodynamic model for wüstite

The wüstite model of Hidayat et al. (2015) considers a solid solution between FeO and $FeO_{1.5}$. The mole fractions of these components are related to the non-stoichiometric factor y of $Fe_{1-y}O$ by

$$X_{FeO_{1.5}} = 2\left(\frac{1}{(1-y)} - 1\right) \tag{A1a}$$

$$X_{FeO} = 1 - X_{FeO_{1.5}} \tag{A1b}$$

The Gibbs free energy of the solution is

$$G = X_{\mathrm{FeO}} G^0_{\mathrm{FeO}} + X_{\mathrm{FeO_{1.5}}} G^0_{\mathrm{FeO_{1.5}}} + \mathrm{R}T\left(X_{\mathrm{FeO}} \ln X_{\mathrm{FeO}} + X_{\mathrm{FeO_{1.5}}} \ln X_{\mathrm{FeO_{1.5}}}\right) + G^{\mathrm{xs}} \tag{A2}$$

where G^{xs} is given by a Bragg-Williams function

$$G^{\mathrm{xs}} = (q_0 + q_1 X_{\mathrm{FeO}}) X_{\mathrm{FeO}} X_{\mathrm{FeO_{1.5}}}, \tag{A3}$$

and values of q_0 and q_1 are −59400 and 42700 J/mole. The activities of components are given by

$$a_i = \gamma_i X_i \tag{S4}$$

for which

$$\mathrm{R}T \ln \gamma_{\mathrm{FeO}} = (q_0 + 2q_1 X_{FeO}) X^2_{\mathrm{FeO_{1.5}}} \tag{S5a}$$

$$\mathrm{R}T \ln \gamma_{\mathrm{FeO_{1.5}}} = X^2_{\mathrm{FeO}} (q_0 + q_1 - 2q_1 X_{\mathrm{FeO_{1.5}}}) \tag{S5b}$$

Values of G_0 at 100 kPa for FeO and $FeO_{1.5}$ are from Hidayat et al. (2015) (Table S1). Extension of endmember free energies to high pressure comes from the expression

$$G^0(T,P) = G^0(T,P_0) + \int_{P_0}^{P} V dP \tag{S6}$$

where P_0 = 100 kPa and the $V\mathrm{d}P$ integral is evaluated numerically at T from the thermal equation of state (EOS) of Komabayashi (2014). The 298 K portion of this EOS is given by a Universal (Vinet) equation

$$P_{298} = 3\frac{K_0}{x^2}(1-x)\exp\left[\frac{3}{2}(K'-1)(1-x)\right], \tag{A7}$$

where K_0 is the bulk modulus (Table S1), $x = (V/V_0)^{1/3}$, V_0 is the volume at 298 K and 100 kPa, and $V(298,P)$ is determined by implicit solution to Eq. A(7). $V(T,P)$ is determined from V(298,P) by

$$V(T,P) = V(298,P) exp(\alpha(T-298)), \tag{A8}$$

where α is

$$\alpha = \alpha_0 exp\left[(-\delta_0/\kappa)\left(1 - \left(\frac{V}{V_0}\right)^{\kappa}\right)\right] \tag{A9}$$

(Komabayashi, 2014). EOS parameters for condensed phases are given in Table S2. MATLAB scripts that uses these relations to calculate the f_{O2} imposed by the IW buffer as a function of pressure and temperature, as well as the predicted equilibrium wüstite composition, are included with the Supplementary data.

VOLUME AND EOS FOR $FEO_{1.5}$ ENDMEMBER OF WÜSTITE

$FeO_{1.5}$ is the fictive oxidized endmember employed in the 100 kPa wüstite thermodynamic model by Hidayat et al. (2015). Volume and other EOS parameters for $FeO_{1.5}$ are required to extend this model to high pressure. Because the $FeO_{1.5}$ composition is well beyond the stability limit of wüstite, these parameters must be extrapolated from wüstites of variable composition.

The volume of $FeO_{1.5}$ at 298 K and 100 kPa, V_0, is derived from the regression shown in Fig. S1. The regression gives V = 12.256+(4.065 ± 0.145)y cm^3/mole on a 1 oxygen basis. Extrapolated to y = 0.3333 and converted to 1.5 oxygens per mole gives V_0 for $FeO_{1.5}$ of 16.372 ± 0.072 cm^3/mole.

A survey of experimentally determined values of K_0 reveals no correlation with wüstite composition (Fig. S2). The best fit line to the K_0 vs. y data, not shown on the plot, has an r^2 of 0.007. Therefore, the value of K_0 for $FeO_{1.5}$ is taken to be 149 GPa, the same as that given for FeO by Komabayashi (2014). This value is not distinguishable from the average of recent (1996–2013) experimental measurements on wüstites of diverse composition (153 ± 6, n = 11). McCammon (1993) suggested that the persistence of non-stoichiometry in wüstite recovered from high pressure multianvil experiments (Fig. 6) may be owing to a larger K_0, near 180 GPa, for FeO-rich compositions. Subsequent work on compositions at or close to stoichiometric FeO (Campbell et al., 2009; Fei, 1996; Haavik et al., 2000; Fischer et al., 2011b) has not supported this conjecture.

APPENDIX B. SUPPLEMENTARY DATA

Supplementary data to this article can be found online at https://doi.org/10.1016/j.gca.2021.08.039.

REFERENCES

Badro J., Fiquet G., Guyot F., Rueff J. P., Struzhkin V. V., Vanko G. and Monaco G. (2003) Iron partitioning in Earth's mantle: Toward a deep lower mantle discontinuity. *Science* **300**, 789–791.

Barr J. A. and Grove T. L. (2010) AuPdFe ternary solution model and applications to understanding the f_{O2} of hydrous, high-pressure experiments. *Contrib. Mineral. Petrol.* **160**, 631–643.

Campbell A. J., Danielson L., Righter K., Seagle C. T., Wang Y. B. and Prakapenka V. B. (2009) High pressure effects on the iron-iron oxide and nickel-nickel oxide oxygen fugacity buffers. *Earth Planet. Sci. Lett.* **286**, 556–564.

Chase M. W. (1998) *NIST-JANAF Themochemical Tables*, 4th ed. American Institute of Physics.

Chipman J. and Marshall S. (1940) The equilibrium $FeO+H_2=Fe+H_2O$ at temperatures up to the melting point of iron. *J. Amer. Chem. Soc.* **62**, 299–305.

Coughlin J. P., King E. G. and Bonnickson K. R. (1951) High-temperature heat contents of ferrous oxide, magnetite and ferric oxide. *J. Amer. Chem. Soc.* **73**, 3891–3893.

Darken L. S. and Gurry R. W. (1945) The system iron oxygen. 1. The wüstite field and related equilibria. *J. Amer. Chem. Soc.* **67**, 1398–1412.

Darken L. S. and Gurry R. W. (1946) The system iron oxygen. 2. Equilibrium and thermodynamics of liquid oxide and other phases. *J. Amer. Chem. Soc.* **68**, 798–816.

Dinsdale A. T. (1991) SGTE data for pure elements. *CALPHAD* **15**, 317–425.

Distin P. A., Whiteway S. G. and Masson C. R. (1971) Solubility of oxygen in liquid iron from 1785° to 1960° C - a new technique for study of slag-metal equilibria. *Canad. Metall. Quart.* **10**, 13–18.

Dorogokupets P. I., Dymshits A. M., Litasov K. D. and Sokolova T. S. (2017) Thermodynamics and equations of state of iron to 350 GPa and 6000 K. *Scientific Reports* **7**, 41863.

Eugster, H.P. (1959) Reduction and oxidation in metamorphism, in: Abelson, P.H. (Ed.), Researches in Geochemistry, pp. 397-426.

Eugster H. P. and Wones D. R. (1962) Stability relations of the ferruginous biotite, annite. *J. Petrol.* **3**, 82–125.

Fabrichnaya O. B. and Sundman B. (1997) The assessment of thermodynamic parameters in the Fe-O and Fe-Si-O systems. *Geochim. Cosmochim. Acta* **61**, 4539–4555.

Fei Y. (1996) Crystal chemistry of FeO at high pressure and temperature. In *Mineral Spectroscopy: A Tribute to Roger G* (eds. M. D. Dyar, C. McCammon and M. W. Shaefer). Burns. Geochemical Society, pp. 243–254.

Fischer R. A., Campbell A. J., Lord O. T., Shofner G. A., Dera P. and Prakapenka V. B. (2011a) Phase transition and metallization of FeO at high pressures and temperatures. *Geophys. Res. Lett.* **38**, L24301.

Fischer R. A., Campbell A. J., Shofner G. A., Lord O. T., Dera P. and Prakapenka V. B. (2011b) Equation of state and phase diagram of FeO. *Earth Planet. Sci. Lett.* **304**, 496–502.

Frost B. R. and Lindsley D. H. (1991) Occurrence of iron-titanium oxides in igneous rocks. *Rev. Mineral.* **25**, 433–468.

Frost D. J., Langenhorst F. and van Aken P. A. (2001) Fe-Mg partitioning between ringwoodite and magnesiowustite and the effect of pressure, temperature and oxygen fugacity. *Phys. Chem. Mineral.* **28**, 455–470.

Frost D. J., Liebske C., Langenhorst F., McCammon C. A., Tronnes R. G. and Rubie D. C. (2004) Experimental evidence for the existence of iron-rich metal in the Earth's lower mantle. *Nature* **428**, 409–412.

Frost D. J., Mann U., Asahara Y. and Rubie D. C. (2008) The redox state of the mantle during and just after core formation. *Phil. Trans. Roy. Soc. A* **366**, 4315–4337.

Frost D. J. and McCammon C. A. (2008) The redox state of Earth's mantle. *Ann. Rev. Earth Planet. Sci.* **36**, 389–420.

Gavarri J.-R. and Carel C. (2019) The complex nonstoichiometry of wustite Fe1-zO: Review and comments. *Prog. Solid State Chem.* **53**, 27–49.

Grove T. L. (1981) Use of FePt alloys to eliminate the iron loss problem in 1-atmosphere gas mixing experiments - theoretical and practical considerations. *Contrib. Mineral. Petrol.* **78**, 298–304.

Haavik C., Stolen S., Hanfland M. and Catlow C. R. A. (2000) Effect of defect clustering on the high-pressure behaviour of wustite. High-pressure X-ray diffraction and lattice energy simulations. *Phys. Chem. Chem. Phys.* **2**, 5333–5340.

Herd C. D. K. (2008) Basalts as probes of planetary interior redox state. *Rev. Mineral. Geochem.* **68**, 527–553.

Hidayat T., Shishin D., Jak E. and Decterov S. A. (2015) Thermodynamic reevaluation of the Fe-O system. *CALPHAD* **48**, 131–144.

Holmström E. and Stixrude L. (2015) Spin Crossover in Ferropericlase from First-Principles Molecular Dynamics. *Phys. Rev. Lett.* **114** 117202.

Jacobsson E. and Rosen E. (1981) Thermodynamic studies of high-temperature equilibria.25. Solid-state EMF studies of the systems Fe-FeO, Ni-NiO and Co-CoO in the temperature-range 1000 K -1600 K. *Scand. J. Metall.* **10**, 39–43.

Kessel R., Beckett J. R. and Stolper E. M. (2001) Thermodynamic properties of the Pt-Fe system. *Am. Mineral.* **86**, 1003–1014.

Komabayashi T. (2014) Thermodynamics of melting relations in the system Fe-FeO at high pressure: Implications for oxygen in the Earth's core. *J. Geophys. Res.* **119**, 4164–4177.

Kowalski M. and Spencer P. J. (1995) Thermodynamic reevaluation of the Cr-O, Fe-O and Ni-O systems - remodeling of the liquid, bcc and fcc phases. *CALPHAD* **19**, 229–243.

Lin J. F., Weir S. T., Jackson D. D., Evans W. J., Vohra Y. K., Qiu W. and Yoo C. S. (2007) *Electrical conductivity of the lower-mantle ferropericlase across the electronic spin transition*. Geophys. Res, Lett, p. 34.

McCammon C. (1993) Effect of pressure on the composition of the lower mantle end member Fe_xO. *Science* **259**, 66–68.

McCammon C. A. and Liu L. G. (1984) The effects of pressure and temperature on nonstoichiometric wüstite, Fe_xO - the iron-rich phase-boundary. *Phys. Chem. Mineral.* **10**, 106–113.

Medard E., McCammon C. A., Barr J. A. and Grove T. L. (2008) Oxygen fugacity, temperature reproducibility, and H_2O contents of nominally anhydrous piston-cylinder experiments using graphite capsules. *Am. Mineral.* **93**, 1838–1844.

Myhill R., Ojwang D. O., Ziberna L., Frost D. J., Ballaran T. B. and Miyajima N. (2016) On the P-T f_{O2} stability of Fe_4O_5, Fe_5O_6 and Fe_4O_5-rich solid solutions. *Contrib. Mineral. Petrol.* **171**, 151.

O'Neill H. S. (1988) Systems Fe-O and Cu-O - Thermodynamic data for the equilibria Fe-FeO, Fe-Fe_3O_4, FeO-Fe_3O_4, Fe_3O_4-Fe_2O_3, Cu-Cu_2O, and Cu_2O-CuO from EMF-measurements. *Am. Mineral.* **73**, 470–486.

O'Neill H. S. and Pownceby M. I. (1993) Thermodynamic data from redox reactions at high-temperatures.1. An experimental and theoretical assessment of the electrochemical method using stabilized zirconia electrolytes, with revised values for the Fe-FeO, Co-CoO, Ni-NiO and Cu-Cu2O oxygen buffers, and new data for the W-WO2 buffer. *Contrib. Mineral. Petrol.* **114**, 296–314.

O'Neill H. S. C., McCammon C. A., Canil D., Rubie D. C., Ross C. R. and Seifert F. (1993) Mössbauer-spectroscopy of mantle transition zone phases and determination of minimum Fe^{3+} content. *Am. Mineral.* **78**, 456–460.

Ohta K., Cohen R. E., Hirose K., Haule K., Shimizu K. and Ohishi Y. (2012) Experimental and theoretical evidence for pressure-induced metallization in FeO with rocksalt-type structure. *Phys. Rev. Lett.* **108** 026403.

Otsuka K., Longo M., McCammon C. A. and Karato S.-I. (2013) Ferric iron content of ferropericlase as a function of composition, oxygen fugacity, temperature and pressure: Implications

for redox conditions during diamond formation in the lower mantle. *Earth Planet. Sci. Lett.* **365**, 7–16.

Ozawa H., Hirose K., Tateno S., Sata N. and Ohishi Y. (2010) Phase transition boundary between B1 and B8 structures of FeO up to 210 GPa. *Phys. Earth. Planet. Int.* **179**, 157–163.

Papike J. J., Karner J. M. and Shearer C. K. (2005) Comparative planetary mineralogy: Valence state partitioning of Cr, Fe, Ti, and V among crystallographic sites in olivine, pyroxene, and spinel from planetary basalts. *Am. Mineral.* **90**, 277–290.

Piet H., Badro J., Nabiei F., Dennenwaldt T., Shim S.-H., Cantoni M., Hebert C. and Gillet P. (2016) Spin and valence dependence of iron partitioning in Earth's deep mantle. *Proc. Nat. Acad. Sci.* **113**, 11127–11130.

Prescher C., Langenhorst F., Dubrovinsky L. S., Prakapenka V. B. and Miyajima N. (2014) The effect of Fe spin crossovers on its partitioning behavior and oxidation state in a pyrolitic Earth's lower mantle system. *Earth Planet. Sci. Lett.* **399**, 86–91.

Rohrbach A., Ballhaus C., Golla-Schindler U., Ulmer P., Kamenetsky V. S. and Kuzmin D. V. (2007) Metal saturation in the upper mantle. *Nature* **449**, 456–458.

Seagle C. T., Heinz D. L., Campbell A. J., Prakapenka V. B. and Wanless S. T. (2008) Melting and thermal expansion in the Fe-FeO system at high pressure. *Earth Planet. Sci. Lett.* **265**, 655–665.

Sjoden O., Seetharaman S. and Staffansson L. I. (1986) On the Gibbs energy of formation of wüstite. *Metall. Trans. B* **17**, 179–184.

Stagno V. and Frost D. J. (2010) Carbon speciation in the asthenosphere: Experimental measurements of the redox conditions at which carbonate-bearing melts coexist with graphite or diamond in peridotite assemblages. *Earth Planet. Sci. Lett.* **300**, 72–84.

Stebbins J. F. and Carmichael I. S. E. (1984) The heat of fusion of fayalite. *Am. Mineral.* **69**, 292–297.

Stølen S. and Grønvold F. (1996) Calculation of the phase boundaries of wüstite at high pressure. *J. Geophys. Res.* **101**, 11531–11540.

Sundman B. (1991) An Assessment of the Fe-O System. *J. Phase Equil.* **12**, 127–140.

Takayama E. and Kimizuka N. (1980) Thermodynamic properties and subphases of wüstite field determined by means of thermogravimetric method in the temperature-range of 1100 °C-1300 °C. *J. Electrochem. Soc.* **127**, 970–976.

Vallet P. and Raccah P. (1964) Sur les limites du domaine de la wüstite solide et le diagramme general qui en resulte. *Comptes Rendus* **258**, 3679–3682.

Wadhwa M. (2008) Redox conditions on small bodies, the Moon and Mars. *Rev. Mineral. Geochem.* **68**, 493–510.

Wriedt H. A. (1991) The Fe-O (Iron-Oxygen) System. *J. Phase Equil.* **12**, 170–200.

Xu S., Lin J.-F. and Morgan D. (2017) Iron partitioning between ferropericlase and bridgmanite in the Earth's lower mantle. *J. Geophys. Res.* **122**, 1074–1087.

Zhang H. L., Hirschmann M. M., Cottrell E. and Withers A. C. (2017) Effect of pressure on Fe^{3+}/SigmaFe ratio in a mafic magma and consequences for magma ocean redox gradients. *Geochim. Cosmochim. Acta* **204**, 83–103.

Associate editor: Bernard Charlier